DYSTONIAS

The HIV protease inhibitor, ritonavir, corrects diverse brain phenotypes across development in mouse model of DYT-TOR1A dystonia

Zachary F. Caffall[1], Bradley J. Wilkes[2], Ricardo Hernández-Martinez[1], Joseph E. Rittiner[1], Jennifer T. Fox[3], Kanny K. Wan[3], Miranda K. Shipman[1], Steven A. Titus[3], Ya-Qin Zhang[3], Samarjit Patnaik[3], Matthew D. Hall[3], Matthew B. Boxer[3], Min Shen[3], Zhuyin Li[3], David E. Vaillancourt[2,4], Nicole Calakos[1,5,6,7]*

Dystonias are a group of chronic movement–disabling disorders for which highly effective oral medications or disease-modifying therapies are lacking. The most effective treatments require invasive procedures such as deep brain stimulation. In this study, we used a high-throughput assay based on a monogenic form of dystonia, DYT1 (DYT-TOR1A), to screen a library of compounds approved for use in humans, the NCATS Pharmaceutical Collection (NPC; 2816 compounds), and identify drugs able to correct mislocalization of the disease-causing protein variant, ΔE302/3 hTorsinA. The HIV protease inhibitor, ritonavir, was among 18 compounds found to normalize hTorsinA mislocalization. Using a DYT1 knock-in mouse model to test efficacy on brain pathologies, we found that ritonavir restored multiple brain abnormalities across development. Ritonavir acutely corrected striatal cholinergic interneuron physiology in the mature brain and yielded sustained correction of diffusion tensor magnetic resonance imaging signals when delivered during a discrete early developmental window. Mechanistically, we found that, across the family of HIV protease inhibitors, efficacy correlated with integrated stress response activation. These preclinical results identify ritonavir as a drug candidate for dystonia with disease-modifying potential.

INTRODUCTION

Dystonias are centrally driven movement disorders characterized by sustained involuntary postures and/or slow twisting movements that lead to motor disability and pain. Presentations range from focal dystonias, affecting single limbs or other body parts, to generalized dystonias where most of the body is involved in abnormal posturing and/or slow uncontrolled twisting movements. Once symptoms manifest, they typically endure throughout an individual's lifetime leading to a notable burden of disability and pain. In all its forms, dystonia is the third most common movement disorder after Parkinson's disease and essential tremor and can arise in many clinical settings—from sporadic and inherited forms to those that occur in association with traumatic brain injury, stroke, neurodegenerative diseases, metabolic disorders, or antipsychotic medication use (*1*, *2*).

There are major unmet treatment needs for dystonia (*2*). The mainstays for oral medication treatment are anticholinergic drugs, benzodiazepines, and muscle relaxants (*2*, *3*). These medications typically reduce the intensity of, but do not eliminate, symptoms (*3*). A narrow therapeutic window further limits their utility. Injectable botulinum toxin is another treatment option, which is used to weaken muscles that are excessively activated (*2*). This approach is helpful when only a few specific muscles are problematic (*2*). Use of this toxin is further limited by the need to maintain some function in muscles, cost, invasiveness, and access to skilled providers to administer the injections. Last, pallidal deep brain stimulation surgery has been shown to be beneficial for some subsets of patients with dystonia, including those with DYT1 dystonia (*4*, *5*). Although encouraging, this is a highly invasive treatment available only at tertiary care centers. Thus, there is a major unmet need for effective, affordable, and easily accessible dystonia treatments.

DYT1 dystonia is an autosomal dominant disease with reduced penetrance that typically presents in childhood and leads to generalized dystonia (*1*, *6*). Symptoms usually begin focally in the first decade of life and progress to involve most of the body over the next several years. The most common causative mutation is an in-frame trinucleotide deletion (n. ΔGAG, p. ΔE) in the *TOR1A* gene that eliminates a glutamic acid residue. The disorder is also thought to have a developmental component because of its childhood onset and because individuals that do not manifest symptoms in the first two decades of life typically never will (*7*). Individuals with DYT1 dystonia can be severely disabled by extensive involuntary movements that interfere with volitional movement control (*2*). Current pharmacological treatments have limited benefits (*8*). Moreover, none of the treatments are disease-modifying (*2*, *3*).

Previously, we developed a high-throughput, high-content (HC) assay for genome-wide RNA interference (RNAi) screening that was based on hTorsinA protein mislocalization caused by the ΔE mutation (*9*). Here, we adapted the assay for chemical library screening to discover potential therapeutics for dystonia. We found that off-target activity of the HIV protease inhibitor (HIV PI), ritonavir, was effective in correcting diverse cellular and brain abnormalities associated with dystonia.

[1]Department of Neurology, Duke University Medical Center, Durham, NC 27715, USA. [2]Department of Applied Physiology and Kinesiology, University of Florida, Gainesville, FL 32611, USA. [3]National Center for Advancing Translational Sciences, National Institutes of Health, Rockville, MD 20850, USA. [4]Department of Neurology, Fixel Institute for Neurological Diseases, McKnight Brain Institute, University of Florida, Gainesville, FL 32611, USA. [5]Department of Neurobiology, Duke University Medical Center, Durham, NC 27715, USA. [6]Department of Cell Biology, Duke University Medical Center, Durham, NC 27715, USA. [7]Duke Institute for Brain Sciences, Duke University, Durham, NC 27715, USA.
*Corresponding author. Email: nicole.calakos@duke.edu

RESULTS

Drug library screen identifies the HIV PI, ritonavir

The mislocalizing propensity of the DYT1 TorsinA protein has been observed in several studies across multiple cell systems (when it is the dominant species, such as in overexpression settings or against a null background) (*9*–*21*). The ΔE TorsinA mislocalizing propensity is also observed independent of whether the protein is expressed as a fusion protein or not (*15*, *16*, *18*, *20*). Recently, this difference in wild-type (WT) and ΔE hTorsinA protein localization was used to develop a high-throughput, high-content assay and successfully applied for genome-wide RNAi screening (*9*). In the screening assay cell lines, a cDNA-expressing enhanced green fluorescent protein (EGFP) fused to the N terminus of hTorsinA is integrated at a defined genomic site in human embryonic kidney (HEK) 293T cells under control of a tetracycline-dependent promotor (Tet-On; fig. S1). EGFP fluorescence is used to monitor the subcellular distribution of the fusion protein. Depending on whether the cell line expresses WT or ΔE hTorsinA, we have previously shown that subcellular distribution markedly differs between a diffuse cytosolic distribution (WT) and punctate pattern (ΔE) (Fig. 1, A and B) (*9*). Automated HC image analysis is used to detect punctate green fluorescence in cells and report the percentage of cells with puncta. To avoid phenotype drift due to selective pressure, EGFP-hTorsinA protein expression is induced at the time of screening by the addition of tetracycline (Fig. 1C). To enable screening of large chemical libraries in dose-response format, assay conditions were adapted to 1536-well plate format. Conditions were identified with a signal window of 7.73 ± 0.69 and a Z′ of 0.67 ± 0.06 in line with recommendations for high-throughput formats (*22*). Because of the potential to translate discoveries to the clinic faster, we screened the NCATS Pharmaceutical Collection (NPC) library, a library of 2816 compounds approved for use in humans. NPC library compounds were assayed in 1536-well

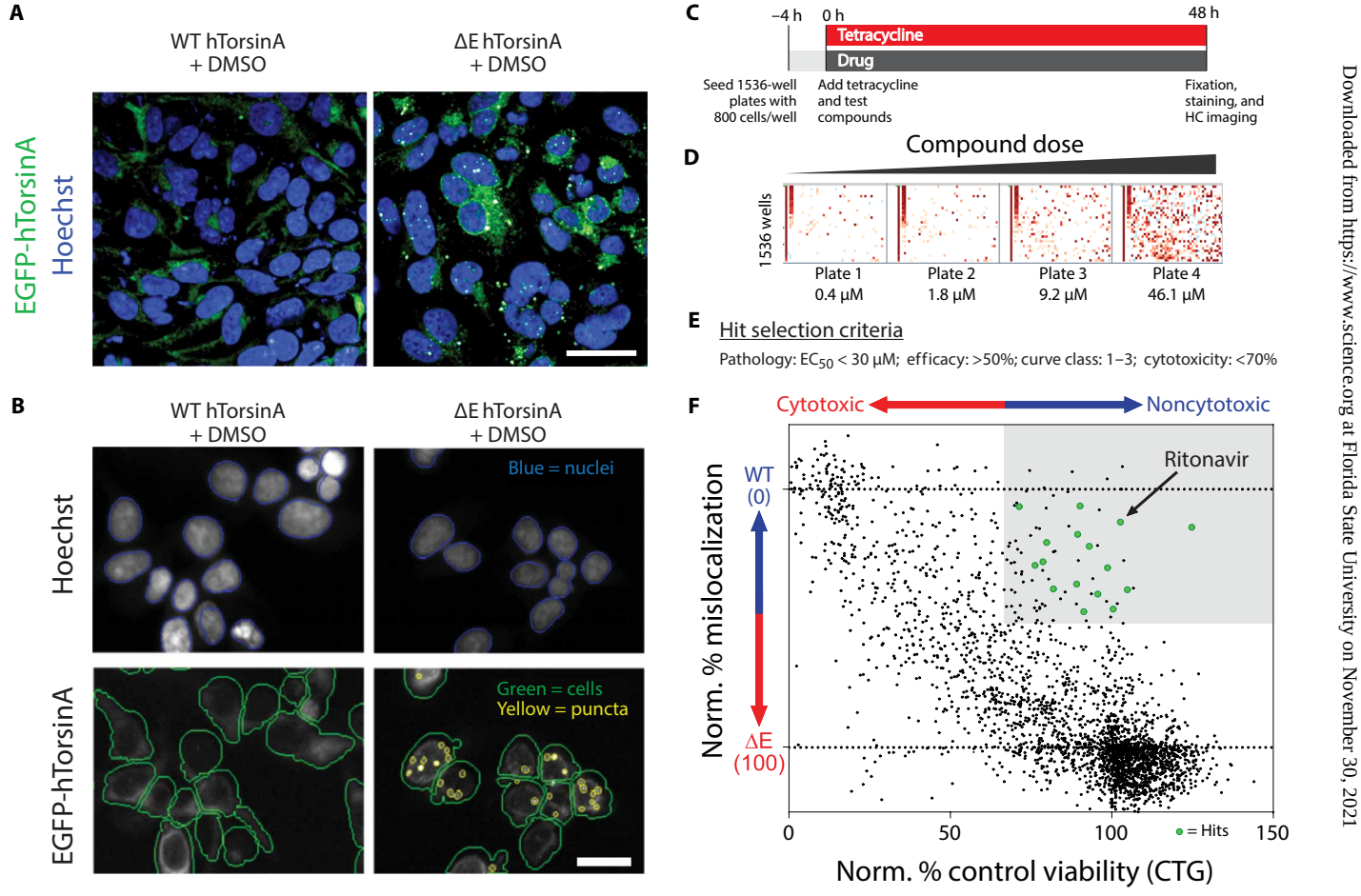

Fig. 1. High-throughput, high-content screen for correction of ΔE hTorsinA protein mislocalization identifies potential therapeutic drugs. (**A**) Representative images of HEK293T assay cell lines after 48 hours of tetracycline-induced EGFP-hTorsinA expression. Scale bar, 40 μm. (**B**) Representative examples of automated image analysis. Cells were identified using nuclear staining (Hoechst). Green fluorescence was used to characterize EGFP-hTorsinA localization as puncta or diffuse. Mislocalization pathology was quantified as the percentage of cells containing EGFP puncta. Scale bar, 20 μm. (**C**) Schematic depicting timeline for high-throughput compound screening assay. (**D**) The NCATS Pharmaceutical Collection (NPC) library was formatted in 1536-well plates with interplate dilutions at four separate doses (0.4, 1.9, 9. 2, and 46.1 μM). Heatmap represents compound performance within wells. (**E**) Criteria for compounds classified as hits. (**F**) Correction of ΔE hTorsinA mislocalization versus cellular viability as measured by CellTiter-Glo (CTG) assay for free ATP (Promega) for each compound tested at 46.08 μM. The percentage of cells containing EGFP puncta was normalized to the range of dimethyl sulfoxide (DMSO)–ΔE cell line representing 100% of this phenotype and DMSO-WT representing 0%. Compounds categorized as hits by criteria in (D) are in green. Gray-shaded box indicates cytotoxicity < 70% (normalized to vehicle-treated ΔE cells = 100) and efficacy of reducing ΔE hTorsinA mislocalization > 50%.

plates with interplate dilutions at four separate doses (0.4, 1.8, 9.2, and 46.1 μM; Fig. 1D). Features of the multitarget analysis module within GE's IN Cell Analysis Investigator Workstation were optimized to quantify the percentage of cells with EGFP puncta (Fig. 1B). Hit selection criteria demanded modest potency and efficacy evidence of a dose-response relationship (curve classes 1 to 3) (*23*), preservation of total EGFP fluorescent intensity and minimal cytotoxicity (Fig. 1E).

Eighteen compounds met these hit selection criteria resulting in an initial hit rate of 0.6% (Fig. 1, E and F). Among these, the HIV PI, ritonavir, stood out because its known target was not present in the assay cell line and off-target mechanisms that had been described in proteostasis (*24*) and the integrated stress response (ISR) (*25*) intersected with processes that are implicated in dystonia pathogenesis (*9*, *26*, *27*).

We performed a series of confirmatory and counter screens to validate the initial hits. In the DYT1 hTorsinA mislocalization assay, new stocks of the 18 hit compounds were obtained and tested in 11-point dose responses from 0.008 to 46.08 μM (figs. S2 and S3). Ten compounds failed to meet dose-response curve, potency, and/or efficacy criteria. To avoid selecting compounds with effects that could derive from interference in the green fluorophore channel, a counter screen was performed using a red fluorescent readout signal (Alexa Fluor 594–conjugated to an anti-GFP antibody). The same 10 compounds that failed in the confirmatory test failed to confirm in this counter screen. Next, we determined whether top hits showed potential to reverse pre-established TorsinA mislocalization by delivering drugs 72 hours after EGFP-ΔE hTorsinA expression induction and assessing effects 12 hours later (fig. S3). Last, an additional four compounds were eliminated because of cytotoxicity using the CellTiter Glo assay (Promega) (table S1). Throughout these additional screens, ritonavir remained among the top performing compounds.

Ritonavir acutely rescues dystonia-associated neurophysiology in brain slices

To vet lead compounds in a more disease-relevant setting, we tested drug effects acutely applied to brain slices ex vivo using a knock-in mouse (*Tor1a*$^{+/\Delta GAG}$) that models the human DYT1 dystonia genotype (*17*). In DYT1 mouse models, abnormalities in dopamine modulation of striatal cholinergic interneurons (SCIs) are reproducibly observed across multiple models and laboratory groups (*28*–*32*). SCIs spontaneously and tonically fire action potentials (*33*). Typically, dopamine through the type 2 dopamine receptor (D2R) causes a reduction in tonic SCI activity (*34*). Paradoxically, in DYT1 mouse models, SCIs respond to D2R agonism with an increase in firing rates rather than decrease (*28*–*32*). This finding has recently been extended to several other dystonia models [DYT-THAP1 (DYT6) and DYT-GNAL (DYT25)], indicating that SCI dysregulation may be a more common feature of dystonia (*35*). In the clinic, anticholinergics are among the more effective dystonia drugs (when tolerated) supporting the plausibility that this phenotype may relate to a pathophysiologically relevant process (*2*, *36*).

To test the ability of ritonavir to rescue the DYT1 SCI phenotype, acute brain slices were preincubated for 1 to 4 hours with vehicle or ritonavir (4 μM) under blinded conditions, and cell-attached recordings of SCIs were performed to assess firing rate modulation by the D2R agonist, quinpirole (10 μM). First, previously described genotype differences in D2R modulation in SCIs of DYT1 knock-in mice were reproduced (Fig. 2, B and C) (*31*, *32*). Next, compared to vehicle preincubation, ritonavir significantly modified the D2R SCI response ($P = 0.0061$), categorically shifting the nature of the modulation back to the WT phenotype of mean rate reduction (<1) rather than augmentation (>1) (Fig. 2, B and C). Measures of SCI intrinsic excitability indicated that ritonavir's effects may occur through modifying action potential kinetics, slowing and widening the action potential waveform (fig. S4). These effects were apparent before quinpirole application and were not further modified by quinpirole exposure. In summary, these results indicate that acute ex vivo exposure of brain tissue to ritonavir is sufficient to normalize the D2R SCI pathophysiology associated with dystonia.

Ritonavir administered during critical developmental period yields long-lasting normalization of DTI MRI

With these encouraging ex vivo results, we aimed to test the effects of ritonavir under systemic and chronic dosing conditions. Ideally, the phenotypic readout would have face validity, such as the dystonia movement disorder itself. However, modeling DYT1 dystonia in rodents has met with limited success in generating a face valid model (*3*, *37*). Genetic perturbations that are more severe than the human clinical setting show proof of principle that ΔE TorsinA can impair movement and cause other severe brain phenotypes (*21*, *38*–*42*). However, because excessive WT TorsinA transgenic overexpression can also cause movement phenotypes and overt cell damage/loss that is beyond the pathology associated with DYT1 dystonia (*42*), we instead chose to maintain the benefits of drug testing in a construct-valid setting that models the causative genotype. For the readout, we selected a brain phenotype that has been described in both human patients and mouse models. Microstructural integrity is disrupted in DYT1 human subjects and knock-in mice. In diffusion tensor imaging (DTI) magnetic resonance imaging (MRI) sequences, both humans and mice show lower fractional anisotropy (FA), a signal that relates to restricted water diffusion in brain tissue, largely attributed to deficits in white matter tracts (*43*–*46*).

To test ritonavir's effects on brain microstructure, we selected an early developmental window for treatment because early development is a period of extensive myelination and microstructural development in both mice and humans (*47*, *48*). In addition, DYT1 dystonia presents in a discrete mid-childhood developmental period. TorsinA expression prominently peaks in early development, and DYT1 mouse models show early developmental time windows for synaptic effects (*7*, *49*–*51*). Because ritonavir is a P-glycoprotein substrate (Pgp, also known as multidrug resistance protein 1) and subject to efflux from the brain, we first performed in vivo pharmacokinetic (PK) studies in young mouse pups with ritonavir and the Pgp inhibitor, elacridar. The combination of ritonavir (15 mg/kg) and elacridar (100 mg/kg) produced brain ritonavir concentrations greater than the screening assay EC_{50} (median effective concentration) for >4 hours (Table 1 and fig. S5) (*52*, *53*). Pregnant dams were treated by intraperitoneal injection from about embryonic day 10 to birth. Pups were treated thereafter using oral gavage until postnatal day 14. Mice were then allowed to reach adulthood ages that have been previously studied with DTI MRI (*43*) before euthanasia and preparation of tissue for ex vivo DTI at 17.6 T.

We performed three types of analysis to test whether ritonavir treatment had a corrective effect on DYT1 genotype–dependent differences in FA. First, we pre-established regions of interest (ROIs) for treatment effects by identifying all voxels with DYT1 genotype–dependent FA differences from WT ($P < 0.05$) in brain areas previously

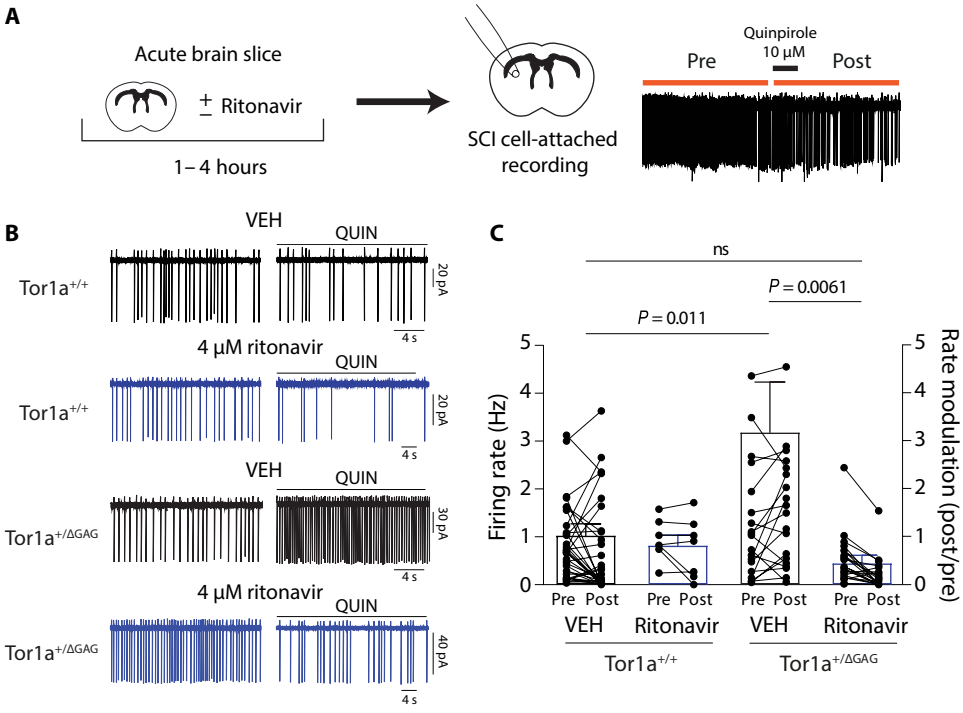

Fig. 2. Ritonavir treatment acutely normalizes dopamine modulation of SCIs in DYT1 knock-in mouse brain slices. (**A**) Illustration of acute ritonavir treatment in brain slice approach and the pause in firing rate normally observed in SCIs after quinpirole (QUIN), a D2R agonist. (**B**) Representative recordings of spontaneous SCI firing in cell-attached configuration before and after the D2R agonist, quinpirole (10μM, 3 min) in WT (*Tor1a*$^{+/+}$) and DYT1 (*Tor1a*$^{+/\Delta GAG}$) brain slices preincubated with ritonavir (4 μM) or vehicle (VEH). (**C**) Quantification showing paired measurements of firing rate before and after quinpirole (dots; left axis) superimposed on summary bar graphs of modulation ratio (post/prefiring rate; right axis) (n = 13 mice, 34 cells WT vehicle; 2 mice, 7 cells WT ritonavir; 7 mice, 19 cells DYT1 vehicle; 7 mice, 23 cells DYT1 ritonavir). P values of two-tailed t test performed on modulation ratios. ns, not significant.

reported to show genotype differences using the same DYT1 mouse model and age (*43*). Previous data have shown that DYT1 mice presented regions of lower FA values within the superior cerebellar tract (R), pons (R), corpus callosum (R), striatum (L), and superior colliculus (R) (Fig. 3B) (*43*). We extracted the genotype-significant voxel subset for each brain area ($P < 0.05$), calculated the mean FA value of those voxels within each area, and performed between-group comparisons for each brain area. Using this approach, four of the five areas previously reported showed significantly lower mean FA values in vehicle-treated DYT1 mice compared to WT controls [$P = 0.0081$ (R) in superior cerebellar tract, $P = 5.4 \times 10^{-4}$ (R) in pons, $P = 0.0032$ (R) in corpus callosum, and $P = 3.3 \times 10^{-4}$ (L) in striatum] (Fig. 3B). Next, within the DYT1 mice, we tested whether ritonavir increased FA values. We found that ritonavir-treated DYT1 mice had significantly higher FA values than vehicle-treated DYT1 mice in three of those four regions [$P = 0.021$ (R) in pons, $P = 0.011$ (R) in corpus callosum, and $P = 2.2 \times 10^{-4}$ (L) in striatum; not (R) superior cerebellar tract ($P = 0.09$)] (Fig. 3B). Last, we found that, in contrast to vehicle-treated DYT1 mice that showed significantly lower FA values than WT in 9 of 10 comparisons made bilaterally in these five brain regions [$P = 0.0032$ (R) and $P = 0.0070$ (L) in corpus callosum, $P = 0.0016$ (R) and $P = 3.3 \times 10^{-4}$ (L) in striatum, $P = 5.4 \times 10^{-4}$ (R) and $P = 0.0014$ (L) in pons, $P = 0.0081$ (R) and $P = 0.0052$ (L) in superior cerebellar tract, and $P = 0.030$ (L) in superior colliculus], ritonavir-treated DYT1 mice failed to show significant differences from WT in FA values in all but 1 of these 10 comparisons [$P = 0.030$ in (R) superior cerebellar tract] (Fig 3B).

To complement this candidate region approach, we also performed whole-brain voxel-wise comparisons between groups. Figure 3C shows representative brain sections with directionality of FA changes noted for all voxels with $P < 0.05$. This analysis indicates that the DYT1 genotype tended to show unidirectional FA differences (lower) brain-wide in comparison to WT (Fig. 3C, left). The comparison between DYT1-ritonavir and WT-vehicle further suggested that normalizing effects of ritonavir may also be more widespread than previously identified ROIs (Fig. 3C, middle). These findings prompted us to consider whether we could use machine learning tools such as support vector machine (SVM) analyses to classify genotype; hence, approaches have been useful in clinical populations with dystonia (*54*). We used SVM to classify brains by genotype using the subset of voxels with $P < 0.05$ for genotype differences (DYT1 versus WT). The SVM model was trained using only the vehicle-treated WT and DYT1 mice and leave-one out (LOO) cross-validation, in which the training occurred on datasets missing a single sample, that was later used as a test subject (Fig. 3D). The receiver operating characteristics for the trained SVM model are shown in fig. S6, and the area under the curve was 0.79. We proceeded to use the genotype-trained SVM classifier to determine whether ritonavir-treated DYT1 mice were classified as DYT1 or WT, using the same subset of voxels. SVM classified 80% (four of five) of the ritonavir-treated DYT1 mice as WT (Fig. 3D). Therefore, each of these distinct analyses provides support that early perinatal treatment of mice with ritonavir causes long-lasting normalizing changes to brain microstructural defects associated with the DYT1 genotype. Together with the neurophysiology results, these animal model studies show corrective effects of ritonavir in DYT1 knock-in mice under diverse treatment conditions—an acute response to ex vivo treatment (Fig. 2) and sustained adulthood effects after chronic dosing in a discrete perinatal window (Fig. 3).

Anti-DYT1 activity and mechanism of HIV PIs

Encouraged by the positive treatment effects of ritonavir on ex vivo and in vivo dystonia-related brain phenotypes, we next sought to understand the mechanism by which ritonavir exerted these effects. First, to determine whether DYT1 hTorsinA assay rescue was unique to ritonavir or shared by other members of the HIV PI class of compounds, we examined the activity of eight U.S. Food and Drug and Administration (FDA)–approved HIV PIs (EC_{50} for HIV protease inhibition ranging from 1 to 80 nM) and one related analog

Table 1. Anti-DYT1 activity of HIV protease inhibitor class of compounds. EC_{50} values shown for data in Figs. 4 and 5. n.d., not determined. Therapeutic window = $\log_2$ of the ratio of EC_{50} for cytotoxicity over localization.

	ΔE hTorsinA mislocalization assay				AARE/ATF4 assay
Collected activity data	**Localization EC_{50} (μM)**	**Localization max efficacy**	**Cytotoxicity EC_{50} (μM)**	**Therapeutic window**	**Pathway activator**
Ritonavir	2.06	97%	44	4.4	Yes
Nelfinavir	3.49	120%	4.2	0.3	Yes
Lopinavir	4.69	70%	37.2	3.0	Yes
Saquinavir	7.52	135%	205.7	4.8	Yes
Deshydroxy-lopinavir	15.98	115%	40.7	1.3	Yes
Cobicistat	17.46	82%	n.d.	n.d.	n.d.
Deshydroxy-ritonavir	37.14	97%	66.2	0.8	n.d.
Atazanavir	No activity		53.3	n.d.	No
Amprenavir	No activity		n.d.	n.d.	No
Darunavir	No activity		n.d.	n.d.	No
Indinavir	No activity		n.d.	n.d.	No

(cobicistat) (Figs. 4 and 5). We found that five of nine HIV PIs reduced ΔE-hTorsinA mislocalization (maximum efficacy, >70% normalization; EC_{50} range, 2 to 16 μM). These results indicate that ritonavir's activity is shared by many but not all HIV PIs. However, of these five, only ritonavir showed good separation of mislocalization effects from cytotoxicity (Fig. 4, A and D). As a drug class, the HIV PIs were developed to inhibit the virally encoded aspartic protease, HIV-1 protease (O90777_9PLVG). Because this protein target is not expressed in the assay cell lines, these results suggest that a common off-target mechanism underlies the dystonia treatment effects that we observe.

We next tested whether a well-known off-target activity of ritonavir could be responsible. Ritonavir inhibits liver and intestinal cytochrome P450 metabolism via inhibition of CYP3A4 (*55*–*57*). The drug cobicistat has two structural modifications from ritonavir that eliminate HIV PI activity while preserving CYP3A4 inhibition (*58*). In the DYT1 hTorsinA mislocalization assay, we found that cobicistat showed more than sevenfold worsening of the EC_{50} compared to ritonavir (Fig. 5). Elimination of the central hydroxyl group (see blue OH in Fig. 5) has also been shown to markedly reduce HIV protease activity without altering CYP3A4 inhibition activity (*58*). We therefore tested the activity of deshydroxy-ritonavir and deshydroxy-lopinavir in the DYT1 hTorsinA mislocalization assay. Compared to ritonavir, deshydroxy-ritonavir showed a more than 10-fold worsening of the EC_{50} (Fig. 5). Similarly, compared to lopinavir, deshydroxy-lopinavir caused a greater than threefold worsening of the EC_{50} (Fig. 4D and Table 1). This series of experiments indicates that CYP3A4 inhibition is unlikely to be the mechanism for anti-DYT1 activity of ritonavir.

Recently, several HIV PIs have been found to stimulate the ISR (*25*). The ISR is a highly conserved signaling network that broadly regulates protein synthesis by eIF2α in settings of cellular stressors as well as learning and memory (*2*, *9*, *59*–*61*). Transcriptional activity of activating transcription factor 4 (ATF4) is a major downstream signaling mechanism for the ISR (*59*). We used a reporter of ATF4 transcriptional activity [amino acid response element (AARE)–dual luciferase; fig. S7] to test whether ISR activation was a feature of HIV PIs with anti-DYT1 activity. Five of nine HIV PIs showed dose-dependent increases in ATF4 transcriptional activity (Fig. 6A). Consistent with our predictions, the five HIV PIs with ATF4 activity were the same compounds that showed efficacy in the DYT1 hTorsinA assay (Fig. 4). However, we also noted that, contrary to the subtler predictions of our hypothesis, the potency for ISR activation and the potency for correction of DYT1 hTorsinA mislocalization were not correlated (fig. S8). For example, of the five compounds, ritonavir had the highest potency for TorsinA localization but the lowest ATF4 transcriptional activity. Ritonavir is also distinguished from the other four compounds because its anti-DYT1 dose-response curve was separable from the cytotoxicity dose-response curve (Fig. 4, A and D). ISR mechanisms can restore cellular homeostasis; however, depending on degree of activation, it can also prompt cellular apoptosis through C/EBP-Homologous Protein (CHOP)–dependent mechanisms (*62*). In this case, we saw that cytotoxicity and ISR activation were strongly correlated (Fig. 6C), whereas autophagy was not activated by HIV PIs (fig. S9). From these experiments, we conclude that ISR activation is a shared property across DYT1-correcting HIV PIs. However, counter to our predictions, among the DYT1-correcting HIV PIs, the degree of ISR activation does not correlate with activity in the dystonia assay but rather with cytotoxicity.

We next sought to directly test whether ISR activity was necessary for ritonavir's activity on DYT1 hTorsinA localization by performing chemical and genetic manipulations that inhibit the ISR (Fig. 6B). ATF4 plays a central role in mediating the cellular response to ISR activation. Previously, we found that expression of an ATF4 cDNA was sufficient to lower DYT1 hTorsinA mislocalization (*9*). Here, using a small interfering RNA (siRNA) knockdown approach, we tested whether inhibiting the ISR pathway by reducing ATF4 expression would lower ritonavir efficacy. In comparison to a nonsilencing control siRNA, ATF4 knockdown significantly lowered ritonavir's efficacy ($P = 5.7 \times 10^{-4}$; Fig. 6D). We also took advantage of a potent and specific tool compound to inhibit the translational consequences of ISR activation, ISRIB (ISR inhibitor) (*63*). Previously, we found that ISRIB alters the normal subcellular localization of WT hTorsinA (*9*). Here, we tested whether ISRIB reduces ritonavir's efficacy in the DYT1 cell line assay. Similar to

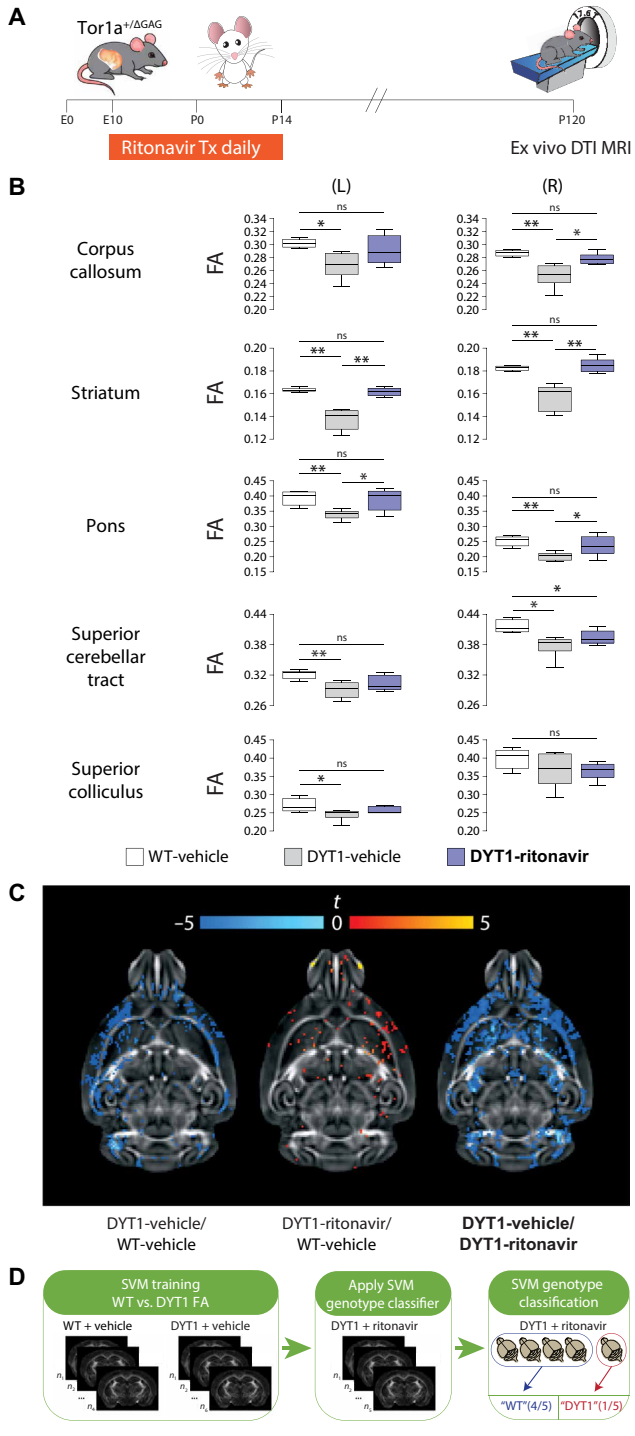

Fig. 3. Daily ritonavir during early development (E10-PND14) corrects DYT1 microstructural abnormalities imaged in adult mice. (**A**) Schematic of experimental design. (**B**) Treatment effects in previously reported genotype-discriminating brain regions of adult *Tor1a* $^{+/\Delta GAG}$ (DYT1) mice; $n = 4$ WT-vehicle, 6 DYT1-vehicle, and 5 DYT1-ritonavir. Box and whiskers plots represent 5 to 95 percentiles. FDR-adjusted one-tailed *t* test; $^{*}P < 0.05$ and $^{**}P < 0.01$. (**C**) Heatmap showing FA values for all voxels reaching $P < 0.05$ by *t* test between indicated groups. (**D**) Support vector machine (SVM) learning algorithm trained on WT-vehicle and DYT1-vehicle voxel-wise FA data that showed genotype differences ($P < 0.05$). SVM classifier was then applied to DYT1-ritonavir, classifying four of five DYT1-ritonavir–treated mice as WT.

observations with ATF4 knockdown, ISR inhibition by ISRIB significantly reduced ritonavir's efficacy ($P = 0.0014$). Last, consistent with prior observations, we noted that, in the vehicle condition, ISRIB increased the percentage of cells with DYT1 hTorsinA mislocalization. From this set of experiments, we conclude that ISR activity contributes to ritonavir's effects.

DISCUSSION

Dystonia is a chronic debilitating disease with a major unmet need for efficacious oral and disease-modifying treatments. In this study, we identify disease-modifying potential for an FDA-approved drug to treat the rare genetic disease, DYT1 early-onset generalized dystonia. The mechanism for ritonavir's effect is independent of its known HIV protease target and involves signaling by the ISR. This drug mechanism intersects with recently described pathophysiology observed across multiple distinct clinical and etiological forms of dystonia (*9*, *64*–*67*), creating the potential for benefit in a substantially larger patient population.

To enable this discovery, a recently described high-content, high-throughput, cell-based screening assay that monitors the punctate mislocalization of EGFP-hTorsinA caused by the DYT1 mutation was adapted for chemical library screening in 1536-well and dose-response format. The NPC of FDA-approved compounds was screened resulting in a 0.6% hit rate, with 18 compounds meeting selection criteria. Ritonavir was among this small number of compounds with high efficacy and potency and low cell toxicity.

Our data suggest that the mechanism for ritonavir in correcting DYT1-related phenotypes is not through its known molecular target, the HIV-1 protease. A number of off-target activities for HIV PIs have been described, and tool compounds isolating HIV protease activity from other effects are available. We found that compounds eliminating the HIV PI activity but preserving off-target activity on cytochrome P450 activity lost efficacy in the DYT1 assay. The recently described off-target activity of HIV PIs intersects directly with a newly proposed mechanism for DYT1 and other dystonias (*25*). We proposed the eIF2α hypothesis for dystonia because phasic activation of the ISR was found to be attenuated in three forms of dystonia (DYT1, DYT16, and sporadic focal), human genetic variants in two pathway genes were associated with dystonia (PRKRA and ATF4), and tool compounds that boosted the ISR showed corrective activity in DYT1 cell and animal models (*9*). Support for this pathway mechanism for dystonia has since extended to other dystonias and is supported by biochemical and human genetic studies from multiple teams (*9*, *64*–*68*). We therefore hypothesized that HIV PIs may correct DYT1-related phenotypes because of their ISR-activating properties. When we explored the potential for ISR activation as a mechanism, we found that ISR activity was common to the subset of HIV PIs with DYT1 assay activity. We also found that chemical and genetic manipulations inhibiting the ISR lowered ritonavir's efficacy.

Modulation of ISR activity state has wide-reaching ramifications for the translated proteome because the ISR causes large shifts in which mRNAs are translated (*59*). The breadth of the impact of ISR modulation on protein abundances might also explain why ritonavir can correct such diverse DYT1-associated phenotypes that may each have distinct molecular underpinnings. In addition, the intersection of corrective mechanisms for HIV PIs and causal mechanisms for dystonia on the ISR indicates potential for ritonavir as a mechanism-targeting therapeutic. Although our findings provide solid support

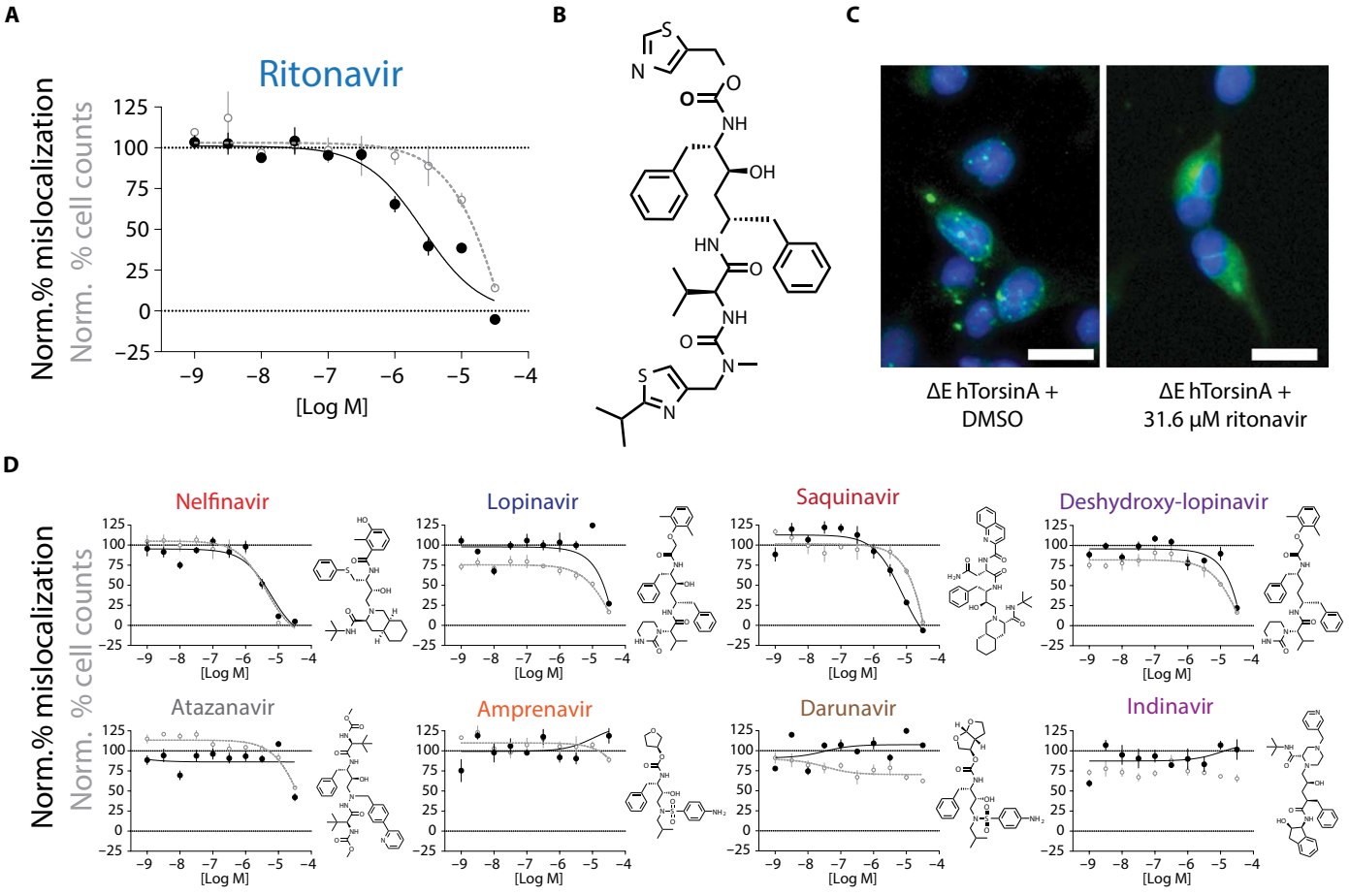

Fig. 4. Activity of HIV PI drugs for normalization of DYT1 hTorsinA mislocalization. (**A**) Dose-response curves for ritonavir on DYT1 hTorsinA localization (black) and cell count (gray) in the ΔE assay cell line. Degree of DYT1 hTorsinA mislocalization was normalized such that vehicle-treated ΔE cells = 100 and vehicle-treated WT cells = 0. Cell count was normalized such that vehicle-treated ΔE cells = 100. (**B**) Structure of the HIV protease inhibitor (PI), ritonavir. (**C**) Representative images from 31.6 μM ritonavir and vehicle treatments in ΔE cell lines. Scale bars, 20 μm. (**D**) Dose-response curves for the family of HIV PI compounds on DYT1 hTorsinA localization (black) and cell count (gray) in the ΔE cell line and their respective structures. $n = 4$ biological replicates per compound dose for dose-response data and 24 for vehicle control data (used for normalization). All data are presented as means ± SEM.

for a contribution of the ISR to ritonavir's effects, we remain open to the possibility that additional mechanisms are involved. Future studies to determine the molecular binding partner of ritonavir will help resolve this important question.

We found that ritonavir was effective in correcting multiple brain phenotypes and under vastly different treatment designs. Ritonavir acutely normalized SCI physiology when applied ex vivo to mature brain slices and also caused long-lasting normalization of DTI MRI signals in adulthood when delivered transiently during a discrete early developmental window. These results show promise for ritonavir or derivatives as potential disease-modifying therapeutics for dystonia. Although neither of these brain phenotypes is dystonia, considerable connections between each of these brain phenotypes and dystonia have been established. Paradoxical SCI firing in response to dopamine (rate increases instead of decreases) has now been described in multiple etiological models of inherited dystonia (*28*–*32*, *35*). Hypercholinergia in the setting of dopamine D2R signaling is further a plausible mechanism for dystonia because among the current best oral medications for children with DYT1 are anticholinergic compounds (but suffer from a poor therapeutic window), and dopamine deficiency (due to genetic loss of function in critical biosynthetic enzymes, dopamine receptor blocking drugs or Parkinson's disease) can cause dystonia. Lower FA (a measure of microstructural integrity in DTI MRI sequences) has now been reported in many forms of dystonia including familial and sporadic disease (*46*, *69*–*74*) and five mouse models involving the *Tor1a* gene (*42*, *43*, *75*–*77*). A few studies further suggest correlations between FA values and dystonia symptomatology (*71*, *78*, *79*). Collectively, these studies support the potential predictive value of the brain readouts tested in this study.

There are several limitations of our study that could influence interpretation and translation to human studies. Most critically, although our study has shown that ritonavir corrects paradoxical SCI firing responses to D2R agonism and white matter deficiencies, we still do not understand how these diverse phenotypes are involved in dystonia disease pathogenesis in humans. To meet success in translation to clinical populations, we see two major milestones ahead. The first concerns determining when in the disease course to administer the drug for the treatment to be effective. The second

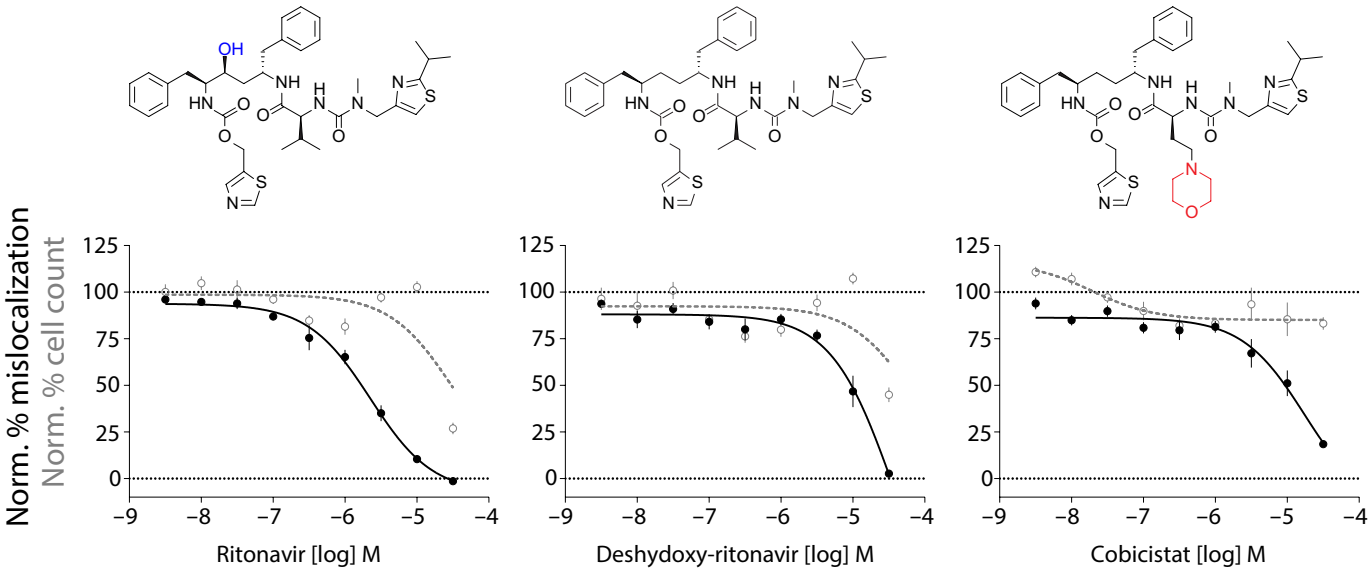

Fig. 5. Ritonavir analogs designed to eliminate HIV PI activity have reduced potency and efficacy. Effect of ritonavir analogs on DYT1 hTorsinA localization (black) and cell count (gray) in the ΔE cell line and their respective structures. Blue and red colors indicate structural differences compared to the intermediate compound, deshydroxy-ritonavir. $n = 4$ per compound dose for dose-response data or 24 for vehicle control data (used for normalization). All data are presented as means ± SEM.

concerns addressing the PK, pharmacodynamic (PD), and risk profile that accompanies using a ritonavir-like molecule at concentrations in the central nervous system (CNS) that are much greater than currently approved indications.

A limitation of our study is that it leaves open the question of when, during the human disease course, a compound like ritonavir should be tested. Because of limitations in preclinical modeling of DYT1 dystonia, we did not have the opportunity to test ritonavir on the movement disorder itself. The DYT1-related brain phenotypes that were corrected by ritonavir support arguments for two very different possibilities: to acutely reverse established symptoms in adulthood and to intervene during a developmental window for sustained benefit without need for ongoing drug treatment in adulthood. We also note that although we showed sufficiency for a brief early developmental treatment period to cause sustained microstructural DTI signal correction, our study design does not rule out the possibility that treatment in the mature adult might also respond. This is an important area for future study. In human studies within and outside of dystonia, the capacity for plasticity of DTI signals has been established (*78*–*80*).

A second major translational issue we anticipate is that, at a minimum, for an indication in dystonia, ritonavir would need to be reformulated to achieve CNS concentrations much higher than those described in the currently approved indications (which suggest at most cerebrospinal fluid concentrations of 2.63 to 32 nM (*52*)). The results in this study were obtained using a dose (15 mg/kg) that achieves peak CNS concentrations of about 5 μM in mice when combined with a Pgp-1 inhibitor. Although these concentrations are much higher than those reported with current ritonavir HIV clinical indications due to unmitigated CNS efflux, the peak plasma and CNS concentrations that we observed at the 15 mg/kg dose in mice are well within the range reported in human plasma (15 μM) under dosing relevant to the HIV clinical indication [600 mg twice daily (BID)] (*81*), as well as the therapeutic window for adverse cytotoxicity suggested both by our data (Table 1) and published studies (*25*, *82*). In this study, we used the Pgp-1 inhibitor tool compound, elacridar, to achieve high CNS concentrations and establish proof of principle. Strategies for CNS delivery will need to be addressed, either through next-generation Pgp inhibitors like zosuquidar (*83*, *84*) or other methods (*85*). Separate from PK/PD and cytotoxicity considerations, there are safety and risk considerations that should be considered when deploying the HIV PI to activate the ISR. The ISR is a fundamental pathway for restoring cellular homeostasis and, when disrupted, in either direction—too much or too little—may have adverse effects (*59*, *60*). Human disorders such as diabetes, dystonia, cancer, Down's syndrome, and traumatic brain injury are just a few examples of diseases in which a causal and/or corrective role for the ISR is involved (*60*). These examples also provide an insight to potential risks. Last, our results across the family of HIV PIs also highlight that the degree of ISR perturbation may crucially influence the clinical suitability of drug candidates. In our study, a drug with modest ISR activity, ritonavir, showed promise in normalizing DYT1 phenotypes, whereas the most potent ISR activator, nelfinavir, suffered from a poor therapeutic window.

In summary, using a recently developed HC, high-throughput screen (HTS) assay that monitors DYT1 hTorsinA mislocalization, we have identified a potentially disease-modifying therapeutic opportunity in the HIV PI, ritonavir. DYT1 is a particularly severe and early-onset form of dystonia in which most of the body can be consumed with involuntary movements that prevent independence with the most basic activities of daily living. Once symptoms onset, usually in early childhood, they are unremitting, exacting a large cumulative toll of disability. There are no well-tolerated, highly effective or disease-modifying oral treatments, and, typically, adequate symptom control requires invasive approaches at specialized tertiary care centers such as botulinum toxin injections and deep brain stimulation. Thus, the availability of an oral drug with disease-modifying potential would transform the current treatment landscape. In addition, DYT1 dystonia is part of a larger group of disorders that include

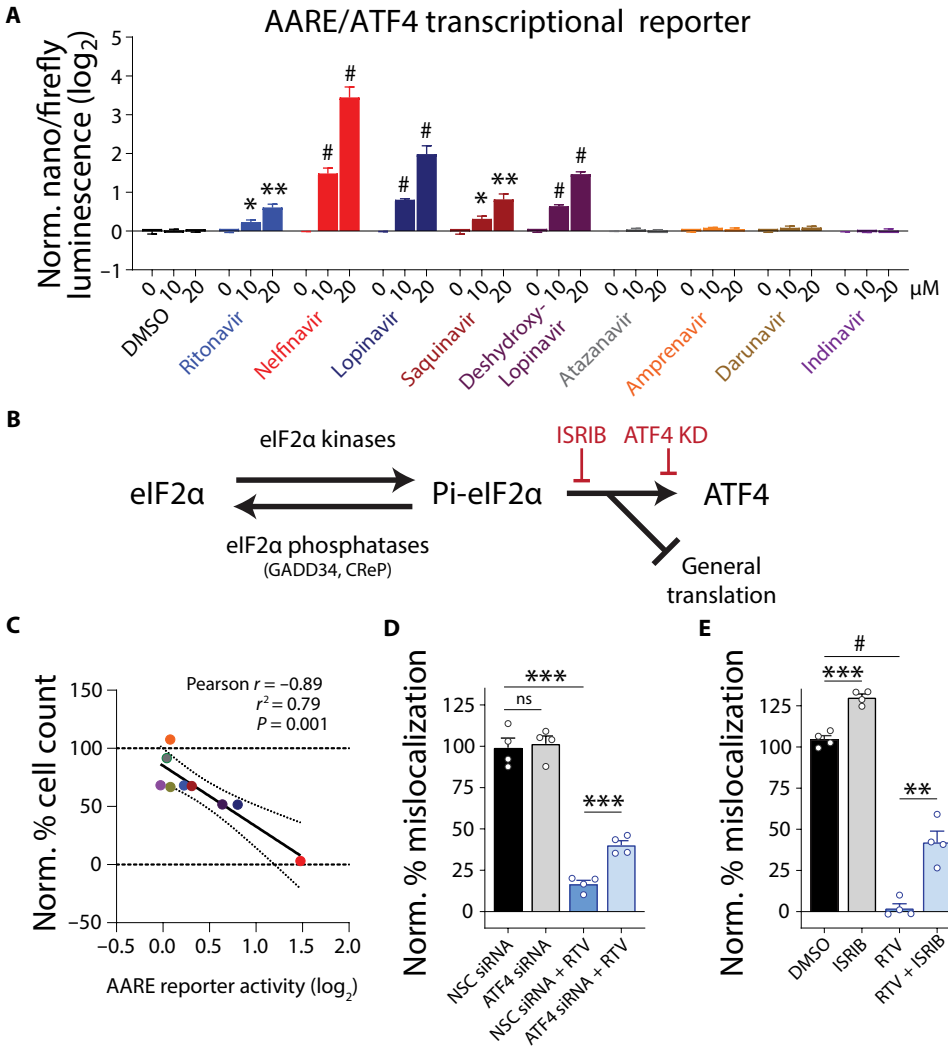

Fig. 6. ISR activation is a characteristic of HIV PI class compounds with anti-DYT1 activity. (**A**) Normalized expression of the AARE/ATF4 luciferase Flp-In 293 dual reporter cell line treated with HIV PIs (at 0, 10, and 20 μM treated for 24 hours). $n = 4$ independent replicates per condition. FDR-corrected two-tailed unpaired t test to DMSO. (**B**) Schematic indicating the sites of chemical and genetic manipulation of the ISR. (**C**) At a 10 μM dose, cytotoxicity correlated with AARE/ATF4 transcriptional reporter activity in the tested HIV PIs. (**D**) DYT1 hTorsinA localization in the ΔE assay cell lines after transfection with ATF4 siRNA. Percent cells with mislocalization were normalized such that nonsilencing control (NSC) siRNA–transfected ΔE cells = 100 and NSC siRNA–transfected WT cells = 0. (**E**) DYT1 hTorsinA localization in the ΔE assay cell lines after treatment with 50 nM ISRIB. Percent cells with mislocalization were normalized such that DMSO-treated ΔE cells = 100 and DMSO-treated WT cells = 0. Ritonavir (RTV) = 10 μM; $n = 4$ wells per condition; two-tailed unpaired t test. $^*P < 0.05$; $^{**}P < 0.01$; $^{***}P < 0.001$; $^{\#}P < 0.0001$. All data are presented as means ± SEM. KD, knockdown. GADD34, growth arrest and DNA-damage-inducible 34. CReP, constitutive repressor of eIF2α phosphorylation.

dystonia and which also lack disease-modifying treatments. The emerging views of multiple forms of dystonia sharing ISR dysfunction suggest possible benefit for dystonias beyond DYT1. The results of the present study showing normalization of diverse dystonia-related brain phenotypes provide strong preclinical support to further consider and develop this class of drugs for dystonia.

MATERIALS AND METHODS

Study design

The objective of this study was to determine the repurposing potential of drugs approved for use in humans as therapeutics for DYT-TOR1A early-onset generalized dystonia. Drug screen: A cell-based, high-content, high-throughput screen was used to test compound efficacy and potency for correction of mislocalization of the causative protein variant, ΔE hTorsinA. A number of replicates for drug screening were established a priori based on assay performance and technical feasibility. Hit calling features were established before screening. Mouse model neurophysiology: Ex vivo slice electrophysiology was used as a secondary assay to test to the ability of ritonavir to acutely correct a previously defined paradoxical increase in firing rate of SCIs in *Tor1a*$^{+/\Delta GAG}$ mice. Adequate sample sizes were identified empirically in pilot studies based on group sizes sufficient to identify genotype differences. Sample sizes were then set as a number of mice per condition based on typical yield of usable cellular recordings. All cells meeting inclusion criteria were used. Exclusion criteria were preestablished, and exclusions (technical recording quality; cell type) were made before unblinding. DTI MRI: Regions in which DTI signal abnormalities had been previously described in dystonia mouse models were chosen before study as an outcome measure for an in vivo preclinical test of ritonavir. Sample sizes were constrained by complexity and limited throughput of experiment and set to have about equal numbers in each group. Analyses were completed before unblinding. SVM analysis was undertaken after recognizing widespread effects of drug treatment. HIV PI mechanistic studies: Chemical and genetic inhibition of the ISR, ISRIB, and ATF4 knockdown were used to confirm the necessity of the ISR for anti-DYT1 activity of ritonavir. For all in vivo and ex vivo studies, primary variable was blinded, and for most studies, genotype was also blinded (WT/DYT1). In vitro mechanistic studies carried out with HC imaging were not blinded but analysis was automated. Datasets do not have any outliers excluded.

Slice electrophysiology

Adult mice (3 to 8 weeks) were anesthetized and intracardially perfused with high-sucrose solution (194 mM sucrose, 30 mM NaCl, 0.2 mM $CaCl_2$, 2 mM $MgCl_2$, 4.5 mM KCl,1.2 mM NaH_2PO_4, 26 mM $NaHCO_3$, and 10 mM glucose, saturated with 95% O_2 and 5% CO_2). Immediately after perfusion, the mice were decapitated, and then brains were dissected and sliced using a Leica VT1200S vibratome (coronal slices; 300 μm). Slices were equilibrated for at least 1 hour in artificial cerebrospinal fluid [ACSF; 124 mM NaCl, 2.5 mM KCl,

10 mM glucose, 2 mM $CaCl_2$, 1 mM $MgCl_2$, 26 mM $NaHCO_3$, and 1.2 mM NaH_2PO_4 saturated with 95% O_2 and 5% CO_2 (pH 7.4), 300 mOsm/liter]. Slices were then superfused continuously in ACSF + 50 μM picrotoxin at 3 to 4 ml/min and 32°C in a recording chamber. Micropipettes were pulled (Narishige pc 100) from borosilicate glass tubes (King Precision Glass) and filled with internal solution [130 mM KSO_4CH_4, 5 mM KCl, 5 mM NaCl, 50 μM $CaCl_2$, 2 mM $MgCl_2$, 10 mM Hepes, 2 mM adenosine triphosphate (ATP)–Mg, 100 μM EGTA, and 400 μM guanosine triphosphate–Na (pH 7.3), 290 mOsm/liter] to achieve a final resistance of 3 to 4.5 megohm. Cholinergic interneurons in the dorsal striatum labeled with enhanced yellow fluorescent protein, visualized using infrared differential interference microscopy, were first recorded in cell-attached mode. After a 15-min baseline recording in ritonavir/vehicle control, 10 μM quinpirole (a selective D2R agonist; Tocris Bioscience) was added to the slice for 3 min, and recording was continued for another 12 min thereafter. Recording was then switched to whole-cell configuration, and electrophysiological properties were used to secondarily identify cell type using the standard current-voltage (I-V) protocol. Drugs were stored as stock solutions and diluted into the perfusion solution, before each experiment, in the final working concentrations indicated. (−)-Quinpirole hydrochloride (10 μM; catalog no. 1061) and ritonavir (4 μM; catalog no. 5856) were from Tocris Bioscience. Picrotoxin (50 μM, CAS 124-87-8) is from Sigma-Aldrich.

DTI MRI acquisition and analysis

Ex vivo DTI acquisition and preprocessing were performed with the same protocol described briefly here (*86*). Mice were perfused with 10% neutral buffered formalin and stored in phosphate-buffered saline before scanning. The skull with encapsulated brain tissue was immersed in FC-40 (Fluorinert) and scanned on an Avance III Bruker 750-MHz (17.6 T) spectrometer at the Advanced Magnetic Resonance Imaging and Spectroscopy facility at University of Florida. Diffusion weighted images were acquired using a two-dimensional diffusion weighted spin echo sequence, with repetition time (TR) = 4.3 s, echo time (TE) = 28 ms, diffusion duration (δ) = 4 ms, diffusion spacing (Δ) = 12 ms, and 3 averages. The voxel resolution was 125-μm^3 isotropic. A total of 60 diffusion directions were used, including 2 b = 0 s/mm^2 volumes, 8 b = 600 s/mm^2 volumes, and 52 b = 3000 s/mm^2 volumes. Total scan time was 22 hours and 47 min. Images were preprocessed using custom Unix shell scripts. Skull stripping was performed on b0 images using PCNN3D in MATLAB (*87*) and ITK-SNAP (*88*) and then applied to all other diffusion volumes. Calculation of FA was performed using DTIFIT in FSL (*89*). Images from each animal were aligned to a common stereotactic space using nonlinear registration with advanced normalization tools (*90*).

Before image analysis and unblinding, ROIs for the superior cerebellar tract, corpus callosum, striatum, and superior colliculus were derived from MRI atlases provided by the Australian Mouse Brain Mapping Consortium (*91*, *92*), and the pons ROI is defined according to the Allen Mouse Brain Atlas (mouse.brain-map.org). We assigned unique labels to ROIs from the left and right hemispheres of the brain. Significant voxels in these ROIs were identified with group comparisons carried out in FSL, using randomized permutation testing with threshold-free cluster enhancement (*93*). We extracted the genotype-significant voxel subset for each ROI, calculated the mean FA value of those voxels within each ROI, and performed between-group comparisons for each ROI. For this ROI analysis, we corrected for multiple comparisons using a 5% false discovery rate (FDR) (*94*). Whole-brain voxel-wise analyses were also performed using FSL Randomise. Whole-brain voxels that differed between veh-DYT1 and WT mice ($P < 0.05$) were saved as a mask, and FA values in those voxels were extracted for each animal. Software functions in MATLAB were used to carry out SVM analysis. The SVM model for binary classification was trained using those FA values from veh-DYT1 and WT mice using LOO cross-validation. The trained SVM model was applied to FA values from ritonavir-DYT1 mice to determine whether they were classified as DYT1 or WT.

Statistical analysis

GraphPad Prism software was used to perform statistical analysis, and all data are shown as means ± SEM unless otherwise indicated in the respective figure legends. Statistical test used, number of replicates, and P value definitions are provided in the respective figure legends. Differences were considered significant when $P < 0.05$.

SUPPLEMENTARY MATERIALS

stm.sciencemag.org/cgi/content/full/13/607/eabd3904/DC1
Materials and Methods
Figs. S1 to S12
Tables S1 and S2
Data file S1
References (*95*–*101*)

View/request a protocol for this paper from *Bio-protocol*.

REFERENCES AND NOTES

1. X. O. Breakefield, A. J. Blood, Y. Li, M. Hallett, P. I. Hanson, D. G. Standaert, The pathophysiological basis of dystonias. *Nat. Rev. Neurosci.* **9**, 222–234 (2008).
2. B. Balint, N. E. Mencacci, E. M. Valente, A. Pisani, J. Rothwell, J. Jankovic, M. Vidailhet, K. P. Bhatia, Dystonia. *Nat. Rev. Dis. Prim.* **4**, 25 (2018).
3. C. Lungu, L. Ozelius, D. Standaert, M. Hallett, B.-A. Sieber, C. Swanson-Fisher, B. D. Berman, N. Calakos, J. C. Moore, J. S. Perlmutter, S. E. Pirio Richardson, R. Saunders-Pullman, L. Scheinfeldt, N. Sharma, R. Sillitoe, K. Simonyan, P. A. Starr, A. Taylor, J. Vitek; participants and organizers of the NINDS Workshop on Research Priorities in Dystonia, Defining research priorities in dystonia. *Neurology* **94**, 526–537 (2020).
4. A. Kupsch, R. Benecke, J. Müller, T. Trottenberg, G.-H. Schneider, W. Poewe, W. Eisner, A. Wolters, J.-U. Müller, G. Deuschl, M. O. Pinsker, I. M. Skogseid, G. K. Roeste, J. Vollmer-Haase, A. Brentrup, M. Krause, V. Tronnier, A. Schnitzler, J. Voges, G. Nikkhah, J. Vesper, M. Naumann, J. Volkmann; Deep-Brain Stimulation for Dystonia Study Group, Pallidal deep-brain stimulation in primary generalized or segmental dystonia. *N. Engl. J. Med.* **355**, 1978–1990 (2006).
5. N. Brüggemann, A. Kühn, S. A. Schneider, C. Kamm, A. Wolters, P. Krause, E. Moro, F. Steigerwald, M. Wittstock, V. Tronnier, A. M. Lozano, C. Hamani, Y.-Y. Poon, S. Zittel, T. Wächter, G. Deuschl, R. Krüger, A. Kupsch, A. Münchau, K. Lohmann, J. Volkmann, C. Klein, Short- and long-term outcome of chronic pallidal neurostimulation in monogenic isolated dystonia. *Neurology* **84**, 895–903 (2015).
6. L. J. Ozelius, S. B. Bressman, Genetic and clinical features of primary torsion dystonia. *Neurobiol. Dis.* **42**, 127–135 (2011).
7. S. B. Bressman, C. Sabatti, D. Raymond, D. de Leon, C. Klein, P. L. Kramer, M. F. Brin, S. Fahn, X. Breakefield, L. J. Ozelius, N. J. Risch, The DYT1 phenotype and guidelines for diagnostic testing. *Neurology* **54**, 1746–1753 (2000).
8. C. C. S. Delnooz, B. P. C. van de Warrenburg, Current and future medical treatment in primary dystonia. *Ther. Adv. Neurol. Disord.* **5**, 221–240 (2012).
9. J. E. Rittiner, Z. F. Caffall, R. Hernández-Martinez, S. M. Sanderson, J. L. Pearson, K. K. Tsukayama, A. Y. Liu, C. Xiao, S. Tracy, M. K. Shipman, P. Hickey, J. Johnson, B. Scott, M. Stacy, R. Saunders-Pullman, S. Bressman, K. Simonyan, N. Sharma, L. J. Ozelius, E. T. Cirulli, N. Calakos, Functional genomic analyses of mendelian and sporadic disease identify impaired eIF2α signaling as a generalizable mechanism for dystonia. *Neuron* **92**, 1238–1251 (2016).
10. D. C. Bragg, S. M. Camp, C. A. Kaufman, J. D. Wilbur, H. Boston, D. E. Schuback, P. I. Hanson, M. Sena-Esteves, X. O. Breakefield, Perinuclear biogenesis of mutant torsin-A inclusions in cultured cells infected with tetracycline-regulated herpes simplex virus type 1 amplicon vectors. *Neuroscience* **125**, 651–661 (2004).
11. A. B. Vander Heyden, T. V. Naismith, E. L. Snapp, D. Hodzic, P. I. Hanson, LULL1 retargets TorsinA to the nuclear envelope revealing an activity that is impaired by the DYT1 dystonia mutation. *Mol. Biol. Cell* **20**, 2661–2672 (2009).

12. F. Vulinovic, K. Lohmann, A. Rakovic, P. Capetian, D. Alvarez-Fischer, A. Schmidt, A. Weißbach, A. Erogullari, F. J. Kaiser, K. Wiegers, A. Ferbert, A. Rolfs, C. Klein, P. Seibler, Unraveling cellular phenotypes of novel TorsinA/TOR1A mutations. *Hum. Mutat.* **35**, 1114–1122 (2014).
13. L. M. Giles, J. Chen, L. Li, L.-S. Chin, Dystonia-associated mutations cause premature degradation of torsinA protein and cell-type-specific mislocalization to the nuclear envelope. *Hum. Mol. Genet.* **17**, 2712–2722 (2008).
14. N. Calakos, V. D. Patel, M. Gottron, G. Wang, K. N. Tran-Viet, D. Brewington, J. L. Beyer, D. C. Steffens, R. R. Krishnan, S. Züchner, Functional evidence implicating a novel TOR1A mutation in idiopathic, late-onset focal dystonia. *J. Med. Genet.* **47**, 646–650 (2010).
15. P. Gonzalez-Alegre, H. L. Paulson, Aberrant cellular behavior of mutant torsinA implicates nuclear envelope dysfunction in DYT1 dystonia. *J. Neurosci.* **24**, 2593–2601 (2004).
16. R. E. Goodchild, W. T. Dauer, Mislocalization to the nuclear envelope: An effect of the dystonia-causing torsinA mutation. *Proc. Natl. Acad. Sci. U.S.A.* **101**, 847–852 (2004).
17. R. E. Goodchild, C. E. Kim, W. T. Dauer, Loss of the dystonia-associated protein torsinA selectively disrupts the neuronal nuclear envelope. *Neuron* **48**, 923–932 (2005).
18. J. Hewett, C. Gonzalez-Agosti, D. Slater, P. Ziefer, S. Li, D. Bergeron, D. J. Jacoby, L. J. Ozelius, V. Ramesh, X. O. Breakefield, Mutant torsinA, responsible for early-onset torsion dystonia, forms membrane inclusions in cultured neural cells. *Hum. Mol. Genet.* **9**, 1403–1413 (2000).
19. J. W. Hewett, F. C. Nery, B. Niland, P. Ge, P. Tan, P. Hadwiger, B. A. Tannous, D. W. Y. Sah, X. O. Breakefield, siRNA knock-down of mutant torsinA restores processing through secretory pathway in DYT1 dystonia cells. *Hum. Mol. Genet.* **17**, 1436–1445 (2008).
20. K. Kustedjo, M. H. Bracey, B. F. Cravatt, Torsin A and its torsion dystonia-associated mutant forms are lumenal glycoproteins that exhibit distinct subcellular localizations. *J. Biol. Chem.* **275**, 27933–27939 (2000).
21. C.-C. Liang, L. M. Tanabe, S. Jou, F. Chi, W. T. Dauer, TorsinA hypofunction causes abnormal twisting movements and sensorimotor circuit neurodegeneration. *J. Clin. Invest.* **124**, 3080–3092 (2014).
22. P. W. Iversen, B. Beck, Y.-F. Chen, W. Dere, V. Devanarayan, B. J. Eastwood, M. W. Farmen, S. J. Iturria, C. Montrose, R. A. Moore, J. R. Weidner, G. S. Sittampalam, HTS Assay Validation (2004).
23. J. Inglese, D. S. Auld, A. Jadhav, R. L. Johnson, A. Simeonov, A. Yasgar, W. Zheng, C. P. Austin, Quantitative high-throughput screening: A titration-based approach that efficiently identifies biological activities in large chemical libraries. *Proc. Natl. Acad. Sci. U.S.A.* **103**, 11473–11478 (2006).
24. P. Andre, M. Groettrup, P. Klenerman, R. de Giuli, B. L. Booth, V. Cerundolo, M. Bonneville, F. Jotereau, R. M. Zinkernagel, V. Lotteau, An inhibitor of HIV-1 protease modulates proteasome activity, antigen presentation, and T cell responses. *Proc. Natl. Acad. Sci. U.S.A.* **95**, 13120–13124 (1998).
25. A. De Gassart, B. Bujisic, L. Zaffalon, L. A. Decosterd, A. Di Micco, G. Frera, R. Tallant, F. Martinon, An inhibitor of HIV-1 protease modulates constitutive eIF2α dephosphorylation to trigger a specific integrated stress response. *Proc. Natl. Acad. Sci. U.S.A.* **113**, E117–E126 (2016).
26. P. Chen, A. J. Burdette, J. C. Porter, J. C. Ricketts, S. A. Fox, F. C. Nery, J. W. Hewett, L. A. Berkowitz, X. O. Breakefield, K. A. Caldwell, G. A. Caldwell, The early-onset torsion dystonia-associated protein, torsinA, is a homeostatic regulator of endoplasmic reticulum stress response. *Hum. Mol. Genet.* **19**, 3502–3515 (2010).
27. A.-Y. Kim, J. B. Seo, W.-T. Kim, H. J. Choi, S.-Y. Kim, G. Morrow, R. M. Tanguay, H. Steller, Y. H. Koh, The pathogenic human Torsin A in *Drosophila* activates the unfolded protein response and increases susceptibility to oxidative stress. *BMC Genomics* **16**, 338 (2015).
28. A. Pisani, G. Martella, A. Tscherter, P. Bonsi, N. Sharma, G. Bernardi, D. G. Standaert, Altered responses to dopaminergic D2 receptor activation and N-type calcium currents in striatal cholinergic interneurons in a mouse model of DYT1 dystonia. *Neurobiol. Dis.* **24**, 318–325 (2006).
29. G. Martella, A. Tassone, G. Sciamanna, P. Platania, D. Cuomo, M. T. Viscomi, P. Bonsi, E. Cacci, S. Biagioni, A. Usiello, G. Bernardi, N. Sharma, D. G. Standaert, A. Pisani, Impairment of bidirectional synaptic plasticity in the striatum of a mouse model of DYT1 dystonia: Role of endogenous acetylcholine. *Brain* **132**, 2336–2349 (2009).
30. G. Sciamanna, R. Hollis, C. Ball, G. Martella, A. Tassone, A. Marshall, D. Parsons, X. Li, F. Yokoi, L. Zhang, Y. Li, A. Pisani, D. G. Standaert, Cholinergic dysregulation produced by selective inactivation of the dystonia-associated protein torsinA. *Neurobiol. Dis.* **47**, 416–427 (2012).
31. G. Martella, M. Maltese, R. Nisticò, T. Schirinzi, G. Madeo, G. Sciamanna, G. Ponterio, A. Tassone, G. Mandolesi, V. Vanni, M. Pignatelli, P. Bonsi, A. Pisani, Regional specificity of synaptic plasticity deficits in a knock-in mouse model of DYT1 dystonia. *Neurobiol. Dis.* **65**, 124–132 (2014).
32. M. Scarduzio, C. N. Zimmerman, K. L. Jaunarajs, Q. Wang, D. G. Standaert, L. L. McMahon, Strength of cholinergic tone dictates the polarity of dopamine D2 receptor modulation of striatal cholinergic interneuron excitability in DYT1 dystonia. *Exp. Neurol.* **295**, 162–175 (2017).
33. B. D. Bennett, J. C. Callaway, C. J. Wilson, Intrinsic membrane properties underlying spontaneous tonic firing in neostriatal cholinergic interneurons. *J. Neurosci.* **20**, 8493–8503 (2000).
34. N. Maurice, J. Mercer, C. S. Chan, S. Hernandez-Lopez, J. Held, T. Tkatch, D. J. Surmeier, D_2 dopamine receptor-mediated modulation of voltage-dependent Na^+ channels reduces autonomous activity in striatal cholinergic interneurons. *J. Neurosci.* **24**, 10289–10301 (2004).
35. K. L. Eskow Jaunarajs, M. Scarduzio, M. E. Ehrlich, L. L. McMahon, D. G. Standaert, Diverse mechanisms lead to common dysfunction of striatal cholinergic interneurons in distinct genetic mouse models of dystonia. *J. Neurosci.* **39**, 7195–7205 (2019).
36. V. Shanker, S. B. Bressman, Diagnosis and management of dystonia. *Continuum (Minneap. Minn).* **22**, 1227–1245 (2016).
37. P. Imbriani, G. Ponterio, A. Tassone, G. Sciamanna, I. El Atiallah, P. Bonsi, A. Pisani, Models of dystonia: An update. *J. Neurosci. Methods* **339**, 108728 (2020).
38. S. S. Pappas, J. Li, T. M. LeWitt, J.-K. Kim, U. R. Monani, W. T. Dauer, A cell autonomous torsinA requirement for cholinergic neuron survival and motor control. *eLife* **7**, e36691 (2018).
39. S. S. Pappas, K. Darr, S. M. Holley, C. Cepeda, O. S. Mabrouk, J. M. T. Wong, T. M. LeWitt, R. Paudel, H. Houlden, R. T. Kennedy, M. S. Levine, W. T. Dauer, Forebrain deletion of the dystonia protein torsinA causes dystonic-like movements and loss of striatal cholinergic neurons. *eLife* **4**, e08352 (2015).
40. F. Richter, A. Bauer, S. Perl, A. Schulz, A. Richter, Optogenetic augmentation of the hypercholinergic endophenotype in DYT1 knock-in mice induced erratic hyperactive movements but not dystonia. *EBioMedicine* **41**, 649–658 (2019).
41. F. Yokoi, M. T. Dang, J. Li, D. G. Standaert, Y. Li, Motor deficits and decreased striatal dopamine receptor 2 binding activity in the striatum-specific Dyt1 conditional knockout mice. *PLOS ONE* **6**, e24539 (2011).
42. K. Grundmann, B. Reischmann, G. Vanhoutte, J. Hübener, P. Teismann, T. K. Hauser, M. Bonin, J. Wilbertz, S. Horn, H. P. Nguyen, M. Kuhn, S. Chanarat, H. Wolburg, A. Van der Linden, O. Riess, Overexpression of human wildtype torsinA and human ΔGAG torsinA in a transgenic mouse model causes phenotypic abnormalities. *Neurobiol. Dis.* **27**, 190–206 (2007).
43. A. M. Uluğ, A. Vo, M. Argyelan, L. Tanabe, W. K. Schiffer, S. Dewey, W. T. Dauer, D. Eidelberg, A. M. Ulug, A. Vo, M. Argyelan, L. Tanabe, W. K. Schiffer, S. Dewey, W. T. Dauer, D. Eidelberg, Cerebellothalamocortical pathway abnormalities in torsinA DYT1 knock-in mice. *Proc. Natl. Acad. Sci. U.S.A.* **108**, 6638–6643 (2011).
44. J. C. DeSimone, M. Febo, P. Shukla, E. Ofori, L. M. Colon-Perez, Y. Li, D. E. Vaillancourt, In vivo imaging reveals impaired connectivity across cortical and subcortical networks in a mouse model of DYT1 dystonia. *Neurobiol. Dis.* **95**, 35–45 (2016).
45. M. Carbon, P. B. Kingsley, S. Su, G. S. Smith, P. Spetsieris, S. Bressman, D. Eidelberg, Microstructural white matter changes in carriers of the DYT1 gene mutation. *Ann. Neurol.* **56**, 283–286 (2004).
46. M. Argyelan, M. Carbon, M. Niethammer, A. M. Ulug, H. U. Voss, S. B. Bressman, V. Dhawan, D. Eidelberg, Cerebellothalamocortical connectivity regulates penetrance in dystonia. *J. Neurosci.* **29**, 9740–9747 (2009).
47. C. Lebel, S. Deoni, The development of brain white matter microstructure. *Neuroimage* **182**, 207–218 (2018).
48. M. Ingalhalikar, D. Parker, Y. Ghanbari, A. Smith, K. Hua, S. Mori, T. Abel, C. Davatzikos, R. Verma, Connectome and maturation profiles of the developing mouse brain using diffusion tensor imaging. *Cereb. Cortex* **25**, 2696–2706 (2015).
49. J. Xiao, S. Gong, Y. Zhao, M. S. LeDoux, Developmental expression of rat torsinA transcript and protein. *Brain Res. Dev. Brain Res.* **152**, 47–60 (2004).
50. A. Vasudevan, X. O. Breakefield, P. G. Bhide, Developmental patterns of torsinA and torsinB expression. *Brain Res.* **1073–1074**, 139–145 (2006).
51. M. Maltese, J. Stanic, A. Tassone, G. Sciamanna, G. Ponterio, V. Vanni, G. Martella, P. Imbriani, P. Bonsi, N. B. Mercuri, F. Gardoni, A. Pisani, Early structural and functional plasticity alterations in a susceptibility period of DYT1 dystonia mouse striatum. *eLife* **7**, e33331 (2018).
52. S. Kravcik, K. Gallicano, V. Roth, S. Cassol, N. Hawley-Foss, A. Badley, D. W. Cameron, Cerebrospinal fluid HIV RNA and drug levels with combination ritonavir and saquinavir. *J. Acquir. Immune Defic. Syndr.* **21**, 371–375 (1999).
53. J. W. Polli, J. L. Jarrett, S. D. Studenberg, J. E. Humphreys, S. W. Dennis, K. R. Brouwer, J. L. Woolley, Role of P-glycoprotein on the CNS disposition of amprenavir (141W94), an HIV protease inhibitor. *Pharm. Res.* **16**, 1206–1212 (1999).
54. Z. Li, C. N. Prudente, R. Stilla, K. Sathian, H. A. Jinnah, X. Hu, Alterations of resting-state fMRI measurements in individuals with cervical dystonia. *Hum. Brain Mapp.* **38**, 4098–4108 (2017).
55. L. L. von Moltke, A. L. Durol, S. X. Duan, D. J. Greenblatt, Potent mechanism-based inhibition of human CYP3A in vitro by amprenavir and ritonavir: Comparison with ketoconazole. *Eur. J. Clin. Pharmacol.* **56**, 259–261 (2000).
56. C. S. Ernest II, S. D. Hall, D. R. Jones, Mechanism-based inactivation of CYP3A by HIV protease inhibitors. *J. Pharmacol. Exp. Ther.* **312**, 583–591 (2005).

57. R. S. Obach, R. L. Walsky, K. Venkatakrishnan, Mechanism-based inactivation of human cytochrome P450 enzymes and the prediction of drug-drug interactions. *Drug Metab. Dispos.* **35**, 246–255 (2007).
58. L. Xu, H. Liu, B. P. Murray, C. Callebaut, M. S. Lee, A. Hong, R. G. Strickley, L. K. Tsai, K. M. Stray, Y. Wang, G. R. Rhodes, M. C. Desai, Cobicistat (GS-9350): A potent and selective inhibitor of human CYP3A as a novel pharmacoenhancer. *ACS Med. Chem. Lett.* **1**, 209–213 (2010).
59. K. Pakos-Zebrucka, I. Koryga, K. Mnich, M. Ljujic, A. Samali, A. M. Gorman, The integrated stress response. *EMBO Rep.* **17**, 1374–1395 (2016).
60. M. Costa-Mattioli, P. Walter, The integrated stress response: From mechanism to disease. *Science* **368**, eaat5314 (2020).
61. A. R. Helseth, R. Hernandez-Martinez, V. L. Hall, M. L. Oliver, B. D. Turner, Z. F. Caffall, J. E. Rittiner, M. K. Shipman, C. S. King, V. Gradinaru, C. Gerfen, M. Costa-Mattioli, N. Calakos, Cholinergic neurons constitutively engage the ISR for dopamine modulation and skill learning in mice. *Science* **372**, eabe1931 (2021).
62. B. F. Teske, M. E. Fusakio, D. Zhou, J. Shan, J. N. McClintick, M. S. Kilberg, R. C. Wek, CHOP induces activating transcription factor 5 (ATF5) to trigger apoptosis in response to perturbations in protein homeostasis. *Mol. Biol. Cell* **24**, 2477–2490 (2013).
63. C. Sidrauski, A. M. McGeachy, N. T. Ingolia, P. Walter, The small molecule ISRIB reverses the effects of eIF2α phosphorylation on translation and stress granule assembly. *eLife* **4**, e05033 (2015).
64. Z. Zakirova, T. Fanutza, J. Bonet, B. Readhead, W. Zhang, Z. Yi, G. Beauvais, T. P. Zwaka, L. J. Ozelius, R. D. Blitzer, P. Gonzalez-Alegre, M. E. Ehrlich, Mutations in THAP1/DYT6 reveal that diverse dystonia genes disrupt similar neuronal pathways and functions. *PLOS Genet.* **14**, e1007169 (2018).
65. L. S. Vaughn, D. C. Bragg, N. Sharma, S. Camargos, F. Cardoso, R. C. Patel, Altered activation of protein kinase PKR and enhanced apoptosis in dystonia cells carrying a mutation in PKR activator protein PACT. *J. Biol. Chem.* **290**, 22543–22557 (2015).
66. D. Mao, C. M. Reuter, M. R. Z. Ruzhnikov, A. E. Beck, E. G. Farrow, L. T. Emrick, J. A. Rosenfeld, K. M. Mackenzie, L. Robak, M. T. Wheeler, L. C. Burrage, M. Jain, P. Liu, D. Calame, S. Küry, M. Sillesen, K. Schmitz-Abe, D. Tonduti, L. Spaccini, M. Iascone, C. A. Genetti, M. K. Koenig, M. Graf, A. Tran, M. Alejandro; Undiagnosed Diseases Network, B. H. Lee, I. Thiffault, P. B. Agrawal, J. A. Bernstein, H. J. Bellen, H.-T. Chao, De novo *EIF2AK1* and *EIF2AK2* variants are associated with developmental delay, leukoencephalopathy, and neurologic decompensation. *Am. J. Hum. Genet.* **106**, 570–583 (2020).
67. C. O. Dos Santos, F. P. da Silva-Júnior, R. D. Puga, E. R. Barbosa, S. M. C. Azevedo Silva, V. Borges, J. C. P. Limongi, M. S. G. Rocha, H. B. Ferraz, P. de Carvalho Aguiar, The prevalence of PRKRA mutations in idiopathic dystonia. *Parkinsonism Relat. Disord.* **48**, 93–96 (2018).
68. G. Beauvais, N. M. Bode, J. L. Watson, H. Wen, K. A. Glenn, H. Kawano, N. C. Harata, M. E. Ehrlich, P. Gonzalez-Alegre, Disruption of protein processing in the endoplasmic reticulum of DYT1 *Knock-in* mice implicates novel pathways in dystonia pathogenesis. *J. Neurosci.* **36**, 10245–10256 (2016).
69. A. Jochim, Y. Li, G. Gora-Stahlberg, T. Mantel, M. Berndt, F. Castrop, C. Dresel, B. Haslinger, Altered functional connectivity in blepharospasm/orofacial dystonia. *Brain Behav.* **8**, e00894 (2018).
70. A. Vo, W. Sako, M. Niethammer, M. Carbon, S. B. Bressman, A. M. Ulug, D. Eidelberg, Thalamocortical connectivity correlates with phenotypic variability in dystonia. *Cereb. Cortex* **25**, 3086–3094 (2015).
71. S. Bianchi, G. Battistella, H. Huddleston, R. Scharf, L. Fleysher, A. F. Rumbach, S. J. Frucht, A. Blitzer, L. J. Ozelius, K. Simonyan, Phenotype- and genotype-specific structural alterations in spasmodic dysphonia. *Mov. Disord.* **32**, 560–568 (2017).
72. M. Carbon, M. Argyelan, D. Eidelberg, Functional imaging in hereditary dystonia. *Eur. J. Neurol.* **17**, 58–64 (2010).
73. L. Bonilha, P. M. de Vries, D. J. Vincent, C. Rorden, P. S. Morgan, M. W. Hurd, N. Besenski, K. J. Bergmann, V. K. Hinson, Structural white matter abnormalities in patients with idiopathic dystonia. *Mov. Disord.* **22**, 1110–1116 (2007).
74. J. Yang, C. Luo, W. Song, X. Guo, B. Zhao, X. Chen, X. Huang, Q. Gong, H.-F. Shang, Diffusion tensor imaging in blepharospasm and blepharospasm-oromandibular dystonia. *J. Neurol.* **261**, 1413–1424 (2014).
75. S. L. Bhagat, S. Qiu, Z. F. Caffall, Y. Wan, Y. Pan, R. M. Rodriguiz, W. C. Wetsel, A. Badea, U. Hochgeschwender, N. Calakos, Mouse model of rare TOR1A variant found in sporadic focal dystonia impairs domains affected in DYT1 dystonia patients and animal models. *Neurobiol. Dis.* **93**, 137–145 (2016).
76. A. Vo, W. Sako, S. L. Dewey, D. Eidelberg, A. M. Uluğ, ^{18}FDG-microPET and MR DTI findings in Tor1a$^{+/-}$ heterozygous knock-out mice. *Neurobiol. Dis.* **73**, 399–406 (2015).
77. J. C. DeSimone, S. S. Pappas, M. Febo, R. G. Burciu, P. Shukla, L. M. Colon-Perez, W. T. Dauer, D. E. Vaillancourt, Forebrain knock-out of torsinA reduces striatal free-water and impairs whole-brain functional connectivity in a symptomatic mouse model of DYT1 dystonia. *Neurobiol. Dis.* **106**, 124–132 (2017).
78. A. J. Blood, J. K. Kuster, J. L. Waugh, J. M. Levenstein, T. J. Multhaupt-Buell, L. R. Sudarsky, H. C. Breiter, N. Sharma, White matter changes in cervical dystonia relate to clinical effectiveness of botulinum toxin treatment. *Front. Neurol.* **10**, 265 (2019).
79. C. Sidiropoulos, S. M. Bowyer, A. Zillgitt, P. A. LeWitt, H. Bagher-Ebadian, E. Davoodi-Bojd, J. M. Schwalb, R. Rammo, E. Air, H. Soltanian-Zadeh, Multimodal imaging in a patient with hemidystonia responsive to GPi deep brain stimulation. *Case Rep. Neurol. Med.* **2017**, 9653520 (2017).
80. C. Sampaio-Baptista, H. Johansen-Berg, White matter plasticity in the adult brain. *Neuron* **96**, 1239–1251 (2017).
81. A. Hsu, G. R. Granneman, R. J. Bertz, Ritonavir. Clinical pharmacokinetics and interactions with other anti-HIV agents. *Clin. Pharmacokinet.* **35**, 275–291 (1998).
82. K. K. Ganta, B. Chaubey, Endoplasmic reticulum stress leads to mitochondria-mediated apoptosis in cells treated with anti-HIV protease inhibitor ritonavir. *Cell Biol. Toxicol.* **35**, 189–204 (2019).
83. A. H. Dantzig, K. L. Law, J. Cao, J. J. Starling, Reversal of multidrug resistance by the P-glycoprotein modulator, LY335979, from the bench to the clinic. *Curr. Med. Chem.* **8**, 39–50 (2001).
84. F. Morschhauser, P. L. Zinzani, M. Burgess, L. Sloots, F. Bouafia, C. Dumontet, Phase I/II trial of a P-glycoprotein inhibitor, Zosuquidar.3HCl trihydrochloride (LY335979), given orally in combination with the CHOP regimen in patients with non-Hodgkin's lymphoma. *Leuk. Lymphoma* **48**, 708–715 (2007).
85. G. D. Kanmogne, S. Singh, U. Roy, X. Liu, J. McMillan, S. Gorantla, S. Balkundi, N. Smith, Y. Alnouti, N. Gautam, Y. Zhou, L. Poluektova, A. Kabanov, T. Bronich, H. E. Gendelman, Mononuclear phagocyte intercellular crosstalk facilitates transmission of cell-targeted nanoformulated antiretroviral drugs to human brain endothelial cells. *Int. J. Nanomedicine* **7**, 2373–2388 (2012).
86. B. J. Wilkes, C. Bass, H. Korah, M. Febo, M. H. Lewis, Volumetric magnetic resonance and diffusion tensor imaging of C58/J mice: Neural correlates of repetitive behavior. *Brain Imaging Behav.* **14**, 2084–2096 (2019).
87. N. Chou, J. Wu, J. Bai Bingren, A. Qiu, K.-H. Chuang, Robust automatic rodent brain extraction using 3-D pulse-coupled neural networks (PCNN). *IEEE Trans. Image Process.* **20**, 2554–2564 (2011).
88. P. A. Yushkevich, J. Piven, H. C. Hazlett, R. G. Smith, S. Ho, J. C. Gee, G. Gerig, User-guided 3D active contour segmentation of anatomical structures: Significantly improved efficiency and reliability. *Neuroimage* **31**, 1116–1128 (2006).
89. M. Jenkinson, C. F. Beckmann, T. E. J. Behrens, M. W. Woolrich, S. M. Smith, FSL. *Neuroimage* **62**, 782–790 (2012).
90. B. B. Avants, P. Yushkevich, J. Pluta, D. Minkoff, M. Korczykowski, J. Detre, J. C. Gee, The optimal template effect in hippocampus studies of diseased populations. *Neuroimage* **49**, 2457–2466 (2010).
91. J. F. P. Ullmann, M. D. Keller, C. Watson, A. L. Janke, N. D. Kurniawan, Z. Yang, K. Richards, G. Paxinos, G. F. Egan, S. Petrou, P. Bartlett, G. J. Galloway, D. C. Reutens, Segmentation of the C57BL/6J mouse cerebellum in magnetic resonance images. *Neuroimage* **62**, 1408–1414 (2012).
92. C. Watson, A. L. Janke, C. Hamalainen, S. M. Bagheri, G. Paxinos, D. C. Reutens, J. F. P. Ullmann, An ontologically consistent MRI-based atlas of the mouse diencephalon. *Neuroimage* **157**, 275–287 (2017).
93. S. M. Smith, T. E. Nichols, Threshold-free cluster enhancement: Addressing problems of smoothing, threshold dependence and localisation in cluster inference. *Neuroimage* **44**, 83–98 (2009).
94. Y. Benjamini, Y. Hochberg, Controlling the false discovery rate: A practical and powerful approach to multiple testing. *J. R. Stat. Soc. Ser. B* **57**, 289–300 (1995).
95. M. E. R. Butchbach, J. D. Edwards, K. R. Schussler, A. H. M. Burghes, A novel method for oral delivery of drug compounds to the neonatal SMNΔ7 mouse model of spinal muscular atrophy. *J. Neurosci. Methods* **161**, 285–290 (2007).
96. M. L. Belleau, R. A. Warren, Postnatal development of electrophysiological properties of nucleus accumbens neurons. *J. Neurophysiol.* **84**, 2204–2216 (2000).
97. Y. Kawaguchi, Large aspiny cells in the matrix of the rat neostriatum in vitro: Physiological identification, relation to the compartments and excitatory postsynaptic currents. *J. Neurophysiol.* **67**, 1669–1682 (1992).
98. Y. Kubota, Y. Kawaguchi, Spatial distributions of chemically identified intrinsic neurons in relation to patch and matrix compartments of rat neostriatum. *J. Comp. Neurol.* **332**, 499–513 (1993).
99. A. Bruhat, C. Jousse, V. Carraro, A. M. Reimold, M. Ferrara, P. Fafournoux, Amino acids control mammalian gene transcription: Activating transcription factor 2 is essential for the amino acid responsiveness of the CHOP promoter. *Mol. Cell. Biol.* **20**, 7192–7204 (2000).
100. K. Pekrun, G. De Alencastro, Q.-J. Luo, J. Liu, Y. Kim, S. Nygaard, F. Galivo, F. Zhang, R. Song, M. R. Tiffany, J. Xu, M. Hebrok, M. Grompe, M. A. Kay, Using a barcoded AAV capsid library to select for clinically relevant gene therapy vectors. *JCI insight* **4**, e131610 (2019).

101. I. F. Sevrioukova, T. L. Poulos, Pyridine-substituted desoxyritonavir is a more potent inhibitor of cytochrome P450 3A4 than ritonavir. *J. Med. Chem.* **56**, 3733–3741 (2013).

Acknowledgments: We thank C. King, T. Greber, A. R. Helseth, and A. Vitenzon for technical assistance. We thank H.-M. Lee, B. L. Roth, and the National Institute of Mental Health Psychoactive Drug Screening Program (University of North Carolina Chapel Hill School of Medicine, Chapel Hill, NC, USA) for piloting initial efforts to adapt screening assay for chemical libraries. We thank W. Zhao and D. Davis for chemistry contributions. We thank the Duke Functional Genomics Shared Resource for technical assistance with high-content screening. **Funding:** This work was supported by Tyler's Hope for a Dystonia Cure Foundation (to N.C.), Harrington Discovery Institute Scholar-Innovator award (to N.C.), Department of Defense PR180747 (to N.C. and M.D.H.), NIH R01 NS075012 (to D.E.V.), the Intramural Research Program of the National Center for Advancing Translational Sciences (NCATS), and partial support from Duke University's CTSA grants UL1 RR024128 and R01 NS075012 (to N.C.). **Author contributions:** Z.F.C., B.J.W., R.H.-M., J.T.F., J.E.R., Z.L., M.D.H., D.E.V., and N.C. designed experiments. J.T.F., M.S., and Y.-Q.Z. performed the HC/HTS. S.A.T. provided HC/HTS imaging expertise. M.S., J.T.F., and Y.-Q.Z. analyzed HC/HTS data. B.J.W. performed DTI-MRI experiments. B.J.W. and D.E.V. analyzed DTI MRI data. R.H.-M. performed slice electrophysiology experiments. M.B.B., K.K.W., and S.P. provided medicinal chemistry expertise. Z.F.C. performed transcriptional reporter experiments. Z.F.C. and M.K.S. performed mislocalization experiments. Z.F.C. performed Western blot experiments. Z.F.C. analyzed all other data. Z.F.C. and N.C. wrote and edited the paper with comments from all authors.

Competing interests: N.C., Z.F.C., J.E.R., M.S., J.T.F., and Z.L. are co-inventors on U.S. patent application no. PCT/US2016/054513 entitled "Compositions and methods for identifying and treating dystonia disorders." N.C., Z.F.C., and J.E.R. are co-inventors on U.S. patent no. 10,857,145. N.C. is a principal investigator on a biomarker research support agreement with Neurocrine Biosciences Inc. and serves in unpaid positions on the Medical and Scientific Advisory Council for the Dystonia Medical Research Foundation and the scientific advisory board for the Collaborative Center for X-Linked Dystonia Parkinsonism at Massachusetts General Hospital. The other authors declare that they have no competing interests. **Data and materials availability:** All data associated with this paper are present in the data file S1 or publically accessible through the PubChem Bioassay repository (PubChem AID 1645839).

Submitted 25 June 2020
Resubmitted 14 December 2020
Accepted 3 June 2021
Published 18 August 2021
10.1126/scitranslmed.abd3904

Citation: Z. F. Caffall, B. J. Wilkes, R. Hernández-Martinez, J. E. Rittiner, J. T. Fox, K. K. Wan, M. K. Shipman, S. A. Titus, Y.-Q. Zhang, S. Patnaik, M. D. Hall, M. B. Boxer, M. Shen, Z. Li, D. E. Vaillancourt, N. Calakos, The HIV protease inhibitor, ritonavir, corrects diverse brain phenotypes across development in mouse model of DYT-TOR1A dystonia. *Sci. Transl. Med.* **13**, eabd3904 (2021).

Science Translational Medicine

The HIV protease inhibitor, ritonavir, corrects diverse brain phenotypes across development in mouse model of DYT-TOR1A dystonia

Zachary F. CaffallBradley J. WilkesRicardo Hernández-MartinezJoseph E. RittinerJennifer T. FoxKanny K. WanMiranda K. ShipmanSteven A. TitusYa-Qin ZhangSamarjit PatnaikMatthew D. HallMatthew B. BoxerMin ShenZhuyin LiDavid E. VaillancourtNicole Calakos

Sci. Transl. Med., 13 (607), eabd3904. • DOI: 10.1126/scitranslmed.abd3904

Tackling dystonia with approved drug

Mutations in *TOR1A* cause a monogenic form of dystonia called DYT1. Patients with DYT1 present chronic movement impairments that persist through life. Effective treatments addressing the cause of the disease are needed. Here, Caffall *et al*. performed in vitro drug screening and in vivo testing to identify potential approved drugs able to normalize the major hallmarks of DYT1. The HIV protease inhibitor, ritonavir, corrected protein mislocalization in vitro and had therapeutic effects in a mouse model of DYT1, ameliorating the phenotype and restoring brain abnormalities when administered during an early postnatal period. The results suggest that this class of drugs might be effective in treating DYT1 by restoring disease-causing cellular abnormalities.